ZKG INTERNATIONAL
ISSN / eISSN 2366-1313
Publisher BAUVERLAG BV GMBH,
AVENWEDDER STR 55, GUTERSLOH, GERMANY, 33311
Volume 25 -Issue 1-(2025)
https://doi.org/10.63386/628914

OPEN ACCESS

Multi-Objective Optimization of Cable Forces in Construction of Long-Span RC Arch Bridges Using Kriging and an Improved Gray Wolf Algorithm

Check for updates

Xuefei Xiong [1], Zheng Cao [2*], Yue Guo [2], Deng Guo [2], Haodong Liu [3], Zhuo Li [2] and Zhongchu Tian [4]

[1] Sichuan Chuanqian Expressway Co., Ltd., Chengdu, Sichuan Province, 610000, China
[2]Sichuan Road & Bridge(Group) Co., Ltd., Chengdu, Sichuan Province, 610000 China
[3] Sichuan Road & Bridge Group Co., Ltd., Chengdu, Sichuan Province, 610000, China
[4] Changsha University of Science & Technology, Changsha, Hunan Province, 410110, China

Corresponding Author: Zheng Cao, Email: chaozheng1990@yeah.net

Abstract: To address the limitations of conventional cable force optimization methods in simultaneously handling multiple objectives, this study presents a Kriging-IGWO multi-objective cable force optimization framework for reinforced concrete (RC) arch bridges, integrated with multi-objective optimization theory. The proposed methodology couples a Kriging surrogate model with an Improved Grey Wolf Optimization (IGWO) algorithm. First, three enhancement strategies are introduced to improve the traditional Grey Wolf Optimizer, reducing its vulnerability to local optima and enabling adaptation to complex high-dimensional optimization problems. Subsequently, the mechanical behavior of RC arch bridges during cantilever construction is analyzed, and a multi-objective cable force optimization model is established using multi-objective theory and the Kriging surrogate model. Finally, the framework is validated through a case study of a long-span RC arch bridge, yielding optimized cable force solutions. The results demonstrate that the IGWO algorithm outperforms other optimization algorithms in convergence accuracy and stabil-ity when solving both unimodal and multimodal test functions. The Kriging-based sur-rogate model for the RC arch bridge meets the required accuracy thresholds and exhibits strong adaptability to multi-objective cable force optimization tasks. The optimized cable force distribution aligns well with the initial design concept but shows a moderate increase in force magnitudes. Notably, peak tensile stresses in the top and bottom slabs of arch segments are significantly reduced, accompanied by decreases in bending moments and axial forces across arch cross-sections. Vertical displacements of the main arch are markedly minimized, and the geometric linearity of the arch is optimized, fully satisfying all predefined design objectives.

Keywords: Reinforced concrete arch bridge; Cable force optimization; Kriging surrogate model; Improving the Gray Wolf algorithm; Multi-Objective optimization

1. Introduction

Characterized by their superior spanning capability, aesthetically pleasing configurations, and exceptional structural durability, reinforced concrete (RC) arch bridges assume a pivotal role in contemporary bridge engineering, finding extensive application in the development of transportation infrastructure, including highways and railways. With the continuous growth of traffic volume and the increasing demands on the structural performance of bridges, ensuring that RC arch bridges have good mechanical properties and stability during their service life has become a key issue in the engineering field. As a critical determinant governing the mechanical behavior of reinforced concrete (RC) arch bridges, the rational optimization of cable forces holds paramount significance. Precise determination of cable force distribution not only enables meticulous modulation of the arch rib's internal force state—thereby maintaining optimal stress levels that balance safety and efficiency under all loading scenarios—but also substantially enhances the bridge's global stiffness, mitigates deformations, and ensures long-term operational reliability throughout its service life.

Conventional cable force optimization methods predominantly rely on finite element analysis (FEA). While delivering high accuracy, these approaches suffer from excessive computational loads and high operational costs, making them impractical for meeting rapid optimization requirements in real-world engineering scenarios [1-3]. Over the past decade, intelligent optimization algorithms have garnered extensive attention and application due to their superior global search capability and effectiveness in handling com-plex problems. Scholars worldwide have begun applying these algorithms to cable force optimization challenges. Zhu [4] employed finite element software and Matlab as the computational core and primary control framework, formulating an objective function centered on minimizing bending moment energy. By integrating an influence matrix and an elite retention strategy into the genetic algorithm, the study conducted optimization of cable forces for the completed-stage cable-stayed bridge. The results demonstrated that this approach could significantly reduce computational workload while attaining superior computational precision. Zhou [5] introduced a cable force optimization methodology

leveraging a deep neural network (DNN) surrogate model. By employing a finite element model to generate load-induced configuration samples that characterize the optimization problem, the DNN surrogate model was utilized to learn the intrinsic mapping relation-ships within these samples—thereby decoupling the optimization process from finite element analysis. Random cable forces within reasonable constraints can be fed into the surrogate model to accurately predict the corresponding arch rib configurations. Zhong [6] utilized an enhanced particle swarm optimization algorithm to optimize the stay cable forces of an asymmetric single-tower cable-stayed bridge in its as-built state. By formulating the objective function as the summation of bending energies for both the main girder and bridge tower, a quadratic mathematical optimization model was established, with outcomes compared against those from the traditional unconstrained minimum bending energy approach. The results demonstrate that the enhanced particle swarm optimization algorithm is efficient, robust, and practically viable for cable force optimization in completed bridge structures. Guo [7] performed an optimization investigation on the cable forces of a specific curved cable-stayed bridge by integrating the simulated annealing algorithm with a cubic B-spline interpolation curve. The results demonstrated that this approach can efficiently generate multiple objective function values, thereby identifying the optimal solution as the minimum among these values and offering a valuable reference for cable force optimization in curved cable-stayed bridge engineering.

Traditional cable force optimization methods are mostly based on a single objective, such as minimizing structural internal forces or only considering the minimization of structural deformation. However, in practical engineering, the optimal design of bridge structures often requires comprehensive consideration of multiple objectives [8-12]. The sole application of machine intelligence algorithms to solve cable force optimization problems suffers from two issues: large computational load and insufficient depth in the practical implementation of such algorithms. Therefore, based on the multi-objective optimization theory, this study combines the improved Gray Wolf algorithm (IGWO) with Kriging surrogate mode to propose a Kriging-IGWO multi-objective cable force optimization method for RC arch Bridges, which can provide references for the cable force optimization of RC arch Bridges in engineering, and has important theoretical significance and engineering application value.

2. Kriging response surface model construction

To fit the response surface of the long-span RC arch bridge, the design parameters of numerous sets of arch bridge models were fed into the finite element software. Subsequently, the corresponding response parameters were acquired. These parameters were then utilized as the training sample dataset for establishing the Kriging surrogate model. Through the establishment of a Kriging surrogate model, the response surface of the RC arch bridge was approximated with high fidelity. Drawing upon the theory of stochastic processes, the Kriging surrogate model forecasts the response of unknown points via the spatial correlation of sample points. This is done to formulate an approximate association between input variables and output responses [12]. Its mathematical representation is presented in Equation (1):

$$y(x) = F(\boldsymbol{\beta}, \mathbf{x}) + z(\mathbf{x}) = \mathbf{f}^T(\mathbf{x})\boldsymbol{\beta} + z(\mathbf{x}) \tag{1}$$

where, $y(x)$ represents the response value of RC arch bridge structure; $\mathbf{f}^T(\mathbf{x})\boldsymbol{\beta}$ stands for the polynomial regression part; $\mathbf{f}(\mathbf{x})$ stands for a polynomial basis function vector; $\boldsymbol{\beta}$ is employed to signify the regression coefficient vector; $z(\mathbf{x})$ is a random part, and its statistical characteristics follow a normal distribution, as presented in equation (2):

$$\begin{aligned} &E(z(x_i)) = 0, D(z(x_i)) = \sigma^2 \\ &Cov[z(x_i), z(x_j)] = \sigma^2 R(\theta, x_i, x_j) \end{aligned} \tag{2}$$

where, θ stands for the correlation function parameter; $R(\theta, x_i, x_j)$ serves as the correlation function between any two sample points. and $d_k = \left|x_i^k - x_j^k\right|$ is usually related, and its expression is shown in equation (3):

$$R(\theta, x_i, x_j) = \prod_{k=1}^{n} R_k(\theta_k, d_k) = \left|x_i^k - x_j^k\right| \tag{3}$$

where, n is the dimension of the random variable.

To precisely acquire the optimal linear unbiased estimation of the prediction point x, it is necessary to minimize the mean square error value of prediction point x, and the expressions of mean and variance are shown in equations (4)-(5):

$$\mu_{\hat{y}}(x) = \hat{\beta} + r(x)R^{-1}(\mathbf{Y} - \beta\hat{F}) \tag{4}$$

$$\sigma^2_{\hat{y}}(x) = \sigma^2(x)(1 + \mu^T(x)(F^T R^{-1} F)^{-1}\mu(x) - r^T(x)R^{-1}r(x)) \tag{5}$$

where, $r(x) = [R(x, x_1; \hat{\theta}), R(x, x_2; \hat{\theta}), \ldots, R(x, x_{N_0}; \hat{\theta})]$, $\mu(x) = F^T R^{-1} r(x) - f(x)$.

The predicted value is:

$$\begin{aligned} \hat{y}(x) &= \mathbf{f}^T\hat{\boldsymbol{\beta}} + \mathbf{r}^T\mathbf{R}^{-1}(\mathbf{Y} - \mathbf{F}\hat{\boldsymbol{\beta}}) \\ \hat{\boldsymbol{\beta}} &= (\mathbf{F}^T\mathbf{R}^{-1}\mathbf{F})^{-1}\mathbf{F}^T\mathbf{R}^{-1}\mathbf{Y} \end{aligned} \tag{6}$$

From the foregoing Kriging model construction procedure, it is evident that the predicted value is exclusively dependent on the variables $\hat{\boldsymbol{\beta}}$, **R** and **r**, so the response value of each sample point can be obtained only by obtaining the relevant parameter θ.

According to equation (1), the stochastic process follows a normal distribution, then $y(x)$ also follows a normal distribution, then the log-likelihood function is:

$$-\frac{1}{2}\left[m\ln\sigma^2 + \ln|\mathbf{R}| + (\mathbf{Y} - \mathbf{F}\hat{\boldsymbol{\beta}})^{\mathbf{T}}\mathbf{R}^{-1}(\mathbf{Y} - \mathbf{F}\hat{\boldsymbol{\beta}}) / \sigma^2 \right] \tag{7}$$

Taking the derivative of $\hat{\boldsymbol{\beta}}$ and σ^2 respectively and substituting them into equation (7), we can get:

$$-\frac{1}{2}\left[m\ln\sigma^2 + \ln|\mathbf{R}| \right] \tag{8}$$

Maximizing equation (8) yields the optimal solution for the parameter θ as follows:

$$\begin{aligned} \theta^* &= \arg\max\left[-\frac{1}{2}\left[m\ln\sigma^2 + \ln|\mathbf{R}| \right] \right] \\ &= \arg\min\left[|\mathbf{R}|^{\frac{1}{m}}\sigma^2 \right] \end{aligned} \tag{9}$$

Kriging prediction model can be constructed by solving the above formula.

3. The improved Gray Wolf algorithm based on multiple strategies

3.1 Standard Gray Wolf algorithm (GWO)

The Grey Wolf Optimizer (GWO), a swarm - based intelligent optimization algorithm, was introduced by Seyedali in 2014. drawing inspiration from the predatory actions and pack hierarchy within grey wolves [13,14]. The rank distribution within the grey wolf population is shown in Figure 1. α wolf is the leader in the grey wolf population, responsible for decision-making on hunting, rest and other group activities, which is consistent with the optimal solution within the optimization problem; β wolf is the assistant of α wolf, assisting in decision - making and guiding the search direction in the algorithm, second only to α wolf, and thus is regarded as the suboptimal solution of the objective function; δ wolf is the third optimal solution of the objective function, which is responsible for reconnaissance and lookout, and plays a role in exploring and developing the search space; ω wolves are at the lowest level of the group, so they should follow the command of other grades of grey wolves and find candidate solutions to the corresponding objective functions in the algorithm [15].

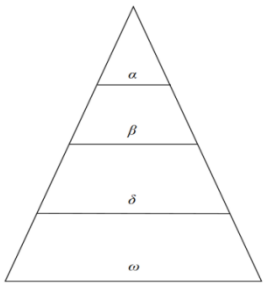

Figure 1 Grey wolf population hierarchy

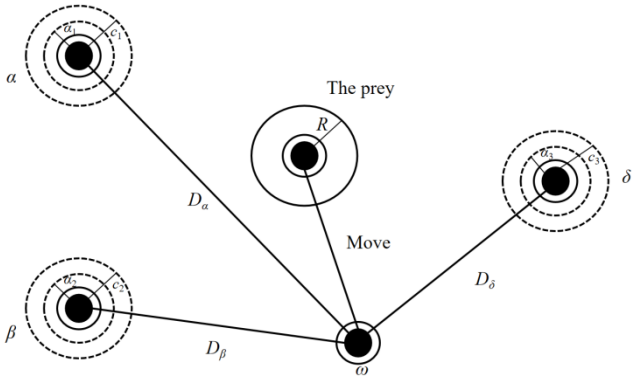

Figure 2 The process of wolf hunting

The optimization process of the GWO algorithm is modeled after the predatory behavior of grey wolf packs. The grey wolf predation process is divided into three sequential stages: prey encirclement, prey pursuit, and prey assault, as illustrated in Figure 2. Guided by the α wolf, β and δ wolves execute prey encirclement, with the prey position assumed to represent the optimal solution. Through iterative approximation by the α, β, and δ wolves—collectively termed the top-tier individuals—the optimal positions of these dominant wolves are leveraged to direct the remaining pack members, including ω wolves, toward continuous convergence on the prey. Within the algorithm's search space, the pack's position update formula during prey encirclement is defined by equation (10):

$$\begin{aligned} \boldsymbol{X}_i(t+1) &= \boldsymbol{X}_p(t) - \boldsymbol{A}\boldsymbol{D} \\ \boldsymbol{D} &= \left|\boldsymbol{C}\boldsymbol{X}_p(t) - \boldsymbol{X}_i(t)\right| \\ \boldsymbol{A} &= 2a\boldsymbol{r}_1 - a \\ \boldsymbol{C} &= 2\boldsymbol{r}_2 \end{aligned} \tag{10}$$

where, t denotes the iteration number in the algorithm; $\boldsymbol{X}_i(t)$ and $\boldsymbol{X}_i(t+1)$ denotes the current location and target location of the gray wolf respectively; $\boldsymbol{X}_p(t)$ denotes the prey position; D is the distance between the first three gray wolves and other wolves; $\boldsymbol{A}$ and $\boldsymbol{C}$ denote the convergence factor vector and the coefficient vector, respectively; $\boldsymbol{r}$ is a random vector with values between 0 and 1; a is the attenuation factor.

Following prey encirclement, the top three wolves (α, β, δ) initiate prey pursuit, leading the entire pack to constrict the encirclement around the prey. The mathematical model describing this hunting process is defined by equation (11):

$$\begin{cases} \boldsymbol{D}_\alpha = \left|\boldsymbol{C}_1\boldsymbol{X}_\alpha(t) - \boldsymbol{X}(t)\right| \\ \boldsymbol{D}_\beta = \left|\boldsymbol{C}_2\boldsymbol{X}_\beta(t) - \boldsymbol{X}(t)\right| \\ \boldsymbol{D}_\delta = \left|\boldsymbol{C}_3\boldsymbol{X}_\delta(t) - \boldsymbol{X}(t)\right| \end{cases} \tag{11}$$

$$\begin{cases} \boldsymbol{X}_1 = \boldsymbol{X}_\alpha(t) - \boldsymbol{A}_1\boldsymbol{D}_\alpha \\ \boldsymbol{X}_2 = \boldsymbol{X}_\beta(t) - \boldsymbol{A}_2\boldsymbol{D}_\beta \\ \boldsymbol{X}_3 = \boldsymbol{X}_\delta(t) - \boldsymbol{A}_3\boldsymbol{D}_\delta \end{cases} \tag{12}$$

$$\boldsymbol{X}'(t+1) = \frac{\boldsymbol{X}_1 + \boldsymbol{X}_2 + \boldsymbol{X}_3}{3} \tag{13}$$

where, $\boldsymbol{D}_\alpha$, $\boldsymbol{D}_\beta$ and $\boldsymbol{D}_\delta$ denote the distances between the top three wolves and individual pack members, respectively; $\boldsymbol{X}_1$, $\boldsymbol{X}_2$ and $\boldsymbol{X}_3$ denote the updated positions of individual pack members based on the positions of the top three wolves; $\boldsymbol{X}'(t+1)$ denotes the final position of an individual wolf after the t-th iteration.

The GWO algorithm computes the fitness values of individual wolves within the pack via iterative updates, thereby enabling the update of their optimal positions. This process enables the continuous optimization of the objective function value and makes it gradually approach the global optimal solution.

3.2 The improved Gray Wolf algorithm

The search mechanism of the traditional GWO algorithm relies on emulating the behavioral patterns of grey wolves with distinct hierarchical roles within the pack. During the algorithm's iterative process, if the α wolf fails to represent the global optimum, its guidance of the search may lead to premature convergence of the population to a local optimum [16-19]. To address this issue, the Levy flight strategy is incorporated into the algorithm to enable individual grey wolves to explore a broader search space, escape local optimum traps, and accelerate convergence. Additionally, to balance the algorithm's local and global search capabilities and enhance its stability, a nonlinear attenuation strategy is employed to adjust the attenuation factor a. Lastly, to enhance the algorithm's search flexibility and improve its convergence performance, a dynamic weight coefficient is incorporated to adjust the grey wolf positions. The detailed improvement procedure is outlined as follows:

In this study, the position of α wolves is updated by employing the Levi flight strategy, and the α wolves guide the other wolves to update the position of the whole population, with the aim of enhancing the algorithm's global search capacity. Levy flight has the characteristics of random and long distance hopping, which can enable the gray wolf donor to explore a larger scope in the search space. Its search step size follows the heavy tail distribution, but the search is more concentrated in the potential area, reducing the search time in the ineffective area. With the incorporation of the Levy flight strategy, the grey wolf position update formula is defined by equation (14):

$$\boldsymbol{X}'(t) = \boldsymbol{X}(t) + l \oplus Levy(\lambda) \tag{14}$$

where, $\boldsymbol{X}'(t)$ denotes the optimal position of a grey wolf after the *t*-th iteration; *l* denotes the weight coefficient; Levy(λ) denotes the search path that obeys the Levy distribution, $\lambda \in (1,3)$,λ in this study is 1.5, so:

$$\begin{cases} r = 0.01\left[\boldsymbol{X}(t) - \boldsymbol{X}_{best}\right] \\ Levy(\lambda) = \dfrac{u}{|v|^{\frac{1}{\lambda}}} \end{cases} \tag{15}$$

where, $\boldsymbol{X}_{best}$ is the historical optimal solution of the algorithm iteration process; *u* and *v* are random variables subject to normal distribution, then:

$$\begin{cases} u \sim N_1(0, \sigma_u^2) \\ v \sim N_2(0, \sigma_v^2) \end{cases}$$

$$\sigma_u = \left\{ \frac{\Gamma(1+\lambda)\sin\frac{\pi\lambda}{2}}{\lambda \cdot \Gamma(\frac{1+\lambda}{2}) \cdot 2^{\frac{\lambda-1}{2}}} \right\} \tag{16}$$

$$\sigma_v = 1$$

where, Γ is a gamma function.

In the Grey Wolf algorithm, the attenuation factor *a* follows a linear attenuation pattern, where its value decreases linearly from 2 to 0 as the number of iterations increases. This linear decay fails to effectively balance the algorithm's global convergence and local search capabilities. To balance the algorithm's local and global search capabilities and enhance its stability, this study proposes a sinusoidal attenuation strategy to modify the linear decay of factor *a* in the GWO algorithm:

$$a = 1 + \sin(\frac{\pi}{2} + \pi \cdot \frac{t}{t_{\max}}) \tag{17}$$

where, $t_{\max}$ denotes the maximum number of iterations in the algorithm.

Figure 3 shows the curves of linear attenuation and sinusoidal attenuation during 100 iterations. From the figure, it is evident that during the algorithm's initial stage, the sinusoidal attenuation factor assumes a larger value, expanding the search range of grey wolf individuals, enhancing global search capabilities, and enabling exploration of the potential optimal solution region within a broader search space. As iterations progress, the sinusoidal attenuation factor decreases nonlinearly, prompting grey wolves to gradually shift focus to local search and exploit high-quality regions, thereby improving solution

accuracy. Therefore, the nonlinear attenuation factor proposed in this study enables better balance between the algorithm's local and global search capabilities.

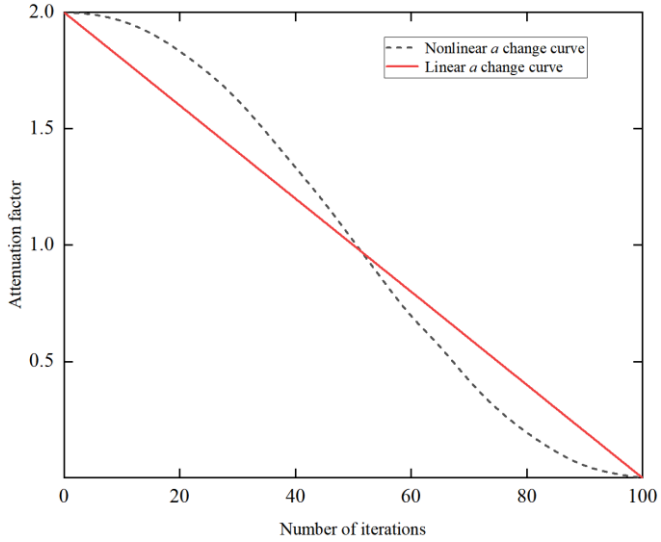

Figure 3 Attenuation factor change curve.

As defined in equation (13), in the traditional GWO algorithm, the final position of each individual wolf is determined as the mean of the top three wolves' positions. Therefore, whether the algorithm can eventually approach the global optimal solution has a close relationship with the positions of the top three - ranked wolves. If the α wolf is not the representative of the global optimal solution, the algorithm has a high probability of landing in the local optimal solution. This study proposes a dynamic weight coefficient strategy to enhance the global optimization capabilities of the GWO algorithm. The dynamic weight coefficient can be adaptively adjusted based on the algorithm's iterative process or search state, enabling individual grey wolves to flexibly switch between exploring new regions and exploiting existing knowledge. This mechanism enhances the algorithm's search flexibility and improves its convergence performance. After introducing the dynamic weight coefficient strategy, the final position of the wolf pack individual after the t iteration is transformed from equation (13) to equation (18), as shown in:

$$\boldsymbol{X}''(t+1)=\frac{\omega_1\boldsymbol{X}_1+\omega_2\boldsymbol{X}_2+\omega_3\boldsymbol{X}_3}{3} \tag{18}$$

$$\begin{cases}\omega_1=\dfrac{\boldsymbol{X}_\alpha}{\boldsymbol{X}_\alpha+\boldsymbol{X}_\beta+\boldsymbol{X}_\delta}\\ \omega_2=\dfrac{\boldsymbol{X}_\beta}{\boldsymbol{X}_\alpha+\boldsymbol{X}_\beta+\boldsymbol{X}_\delta}\\ \omega_3=\dfrac{\boldsymbol{X}_\delta}{\boldsymbol{X}_\alpha+\boldsymbol{X}_\beta+\boldsymbol{X}_\delta}\end{cases} \tag{19}$$

where, *w* denotes the weight coefficient for the positions of the top three wolves;
The flow of the IGWO algorithm is depicted in Figure 4.

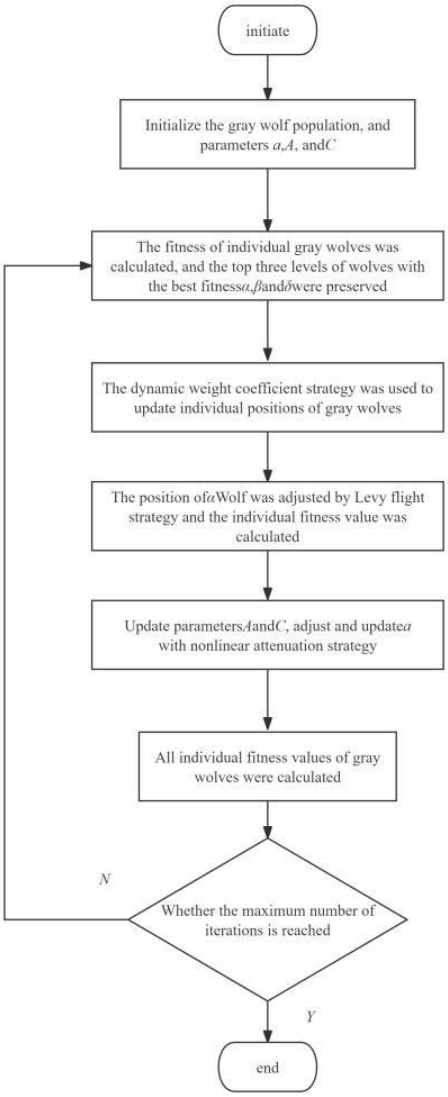

Figure 4 IGWO algorithm flowchart.

4. Multi-objective cable force optimization model in Kriging-IGWO

To determine the optimal cable force combination during the cantilever construction of an RC arch bridge, this study aims to ensure reasonable load distribution after the bridge is completed, control its deformation under service loads, and safeguard the structural safety of the arch bridge. This study establishes a cable force optimization model grounded in Kriging-IGWO. Taking the arch bridge's design cable forces as design variables, the model defines the optimization control goals as the stress of the arch ring section during the cantilever construction stage, the internal forces of the completed arch bridge, and its deformation.

During the cantilever construction stage of an RC arch bridge, the stress distribution in the arch ring section is relatively complex, where excessive tensile stress during cable force adjustment can easily lead to cracks in the top and bottom flanges of the arch ring. Therefore, to ensure that the tensile stress in the arch ring does not exceed the concrete's tensile strength during cable force tensioning, the average tensile stress at the top and bottom flanges of the arch ring is set as the control objective, and the optimization objective function is formulated as follows:

$$O_1 = \mathrm{Min}\left[\frac{1}{n}\sum_{i=1}^{n}\left(\sigma_i^t + \sigma_i^b\right)\right] \tag{20}$$

where, n denotes the quantity of cantilever pouring stages for the RC arch bridge; σ denotes the tensile stress in the arch ring during the cantilever pouring stage of an RC arch bridge;

Optimizing the cable forces of the stay cables in an RC arch bridge leads to a more reasonable internal force distribution in the bridge's main load-bearing components. This optimization enables full utilization of material properties and enhances the load-bearing capacity of the bridge structure. By taking the eccentric moment of the bridge's main arch as the control objective for its internal forces, the optimization objective function is formulated as follows:

$$O_2 = \mathrm{Min}\left[\sum_{i=1}^{n}\frac{|e_i|}{n}\right] \tag{21}$$

where, e is the eccentricity of the main arch, $e_i = M_i / N_i$.

Optimizing the cable forces of an RC arch bridge effectively controls its deformation under dead weight and service loads, ensuring that the bridge's linear geometry better meets the design specifications. Taking the sum of squares of the differences between the vertical displacements obtained from finite element calculations and the target vertical displacements at each construction stage of the completed arch ring as the deformation control objective, the optimization objective function is formulated as follows:

$$O_3 = \mathrm{Min}\left[\frac{1}{n}\sum_{i=1}^{n}(u_i - \hat{u}_i)^2\right] \tag{22}$$

Based on the cable force design, 50 groups of sample points were selected by Latin hypercube and calculated in the finite element software. The response values of the above control targets were obtained, and the response values were substituted into the Kriging model for fitting. To check the prediction accuracy of Kriging surrogate mode, this study uses the complex correlation coefficient R^2 to illustrate. The closer R^2 is to 1, the higher the accuracy of the model [18-22].

$$R^2 = \frac{\sum_{i=1}^{n}(\mu_{i,pre} - \mu_{ave})^2}{\sum_{i=1}^{n}(\mu_{i,true} - \mu_{ave})^2} \tag{23}$$

where, $\mu_{i,pre}$, $\mu_{i,true}$ and μ_{ave} denote the predicted value, true value, and average value of point i, respectively.

Based on the above analysis, a cable force optimization model for RC arch bridges under cantilever casting was established using Kriging-IGWO. According to the principle of symmetrical structure, 21 stay cables of half structure were selected for analysis. The optimized mathematical model is shown in Equation (24).

$$\begin{aligned} &\text{Find} \quad X = [x_1, x_2, \cdots, x_{21}]^T \\ &\min(O_1, O_2, O_3) \\ &\text{s.t.}\begin{cases} \sigma_i \le f_i^t \\ e_i \le \dfrac{2I_i}{A_i H_i} \\ u \le u_i - \hat{u}_i \le \bar{u} \end{cases} \end{aligned} \tag{24}$$

where, $\boldsymbol{X}$ denotes the cable force to be optimized; f_i^t denotes the design tensile strength of the concrete in an RC arch bridge..

Figure 5 depicts the fundamental workflow of cable force optimization for the Kriging-IGWO-based RC arch bridge structure during cantilever pouring construction.

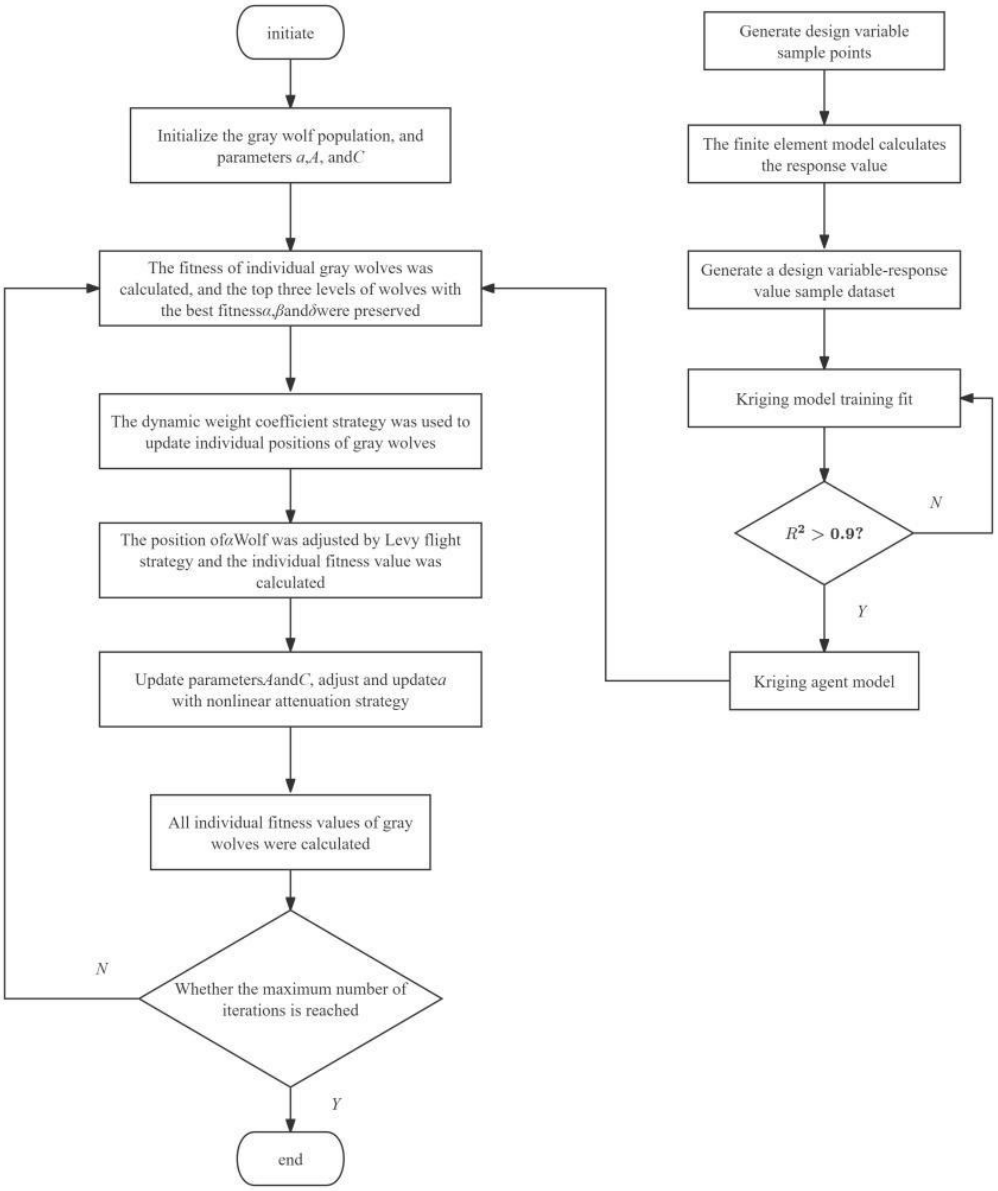

Figure 5 Cable force optimization process of RC arch bridge based on Kriging-IGWO.

5. Engineering Example

5.1 Engineering background and finite element model

Against the project background of the Shuiluohe Bridge in Guizhou Province, the main bridge is a reinforced concrete cantilever-cast arch bridge with a calculated span of 335 m. The main bridge deck consists of simply supported prestressed concrete I-beams with a span arrangement of 11×31.75 m and composite bridge panels. A catenary unhinged arch of the same cross - section is employed for the main arch. The ratio of its vector span is 1/4.2, while the coefficient of the arch axis is 1.8. The arch rib is constructed in 45 sections, and section 1-2 (1 '~2') of arch foot is cast in place by scaffolding. Section 3-22 (3 '~22') adopts hanging basket cantilever casting, and mid-span closing section adopts hanger construction. C80 concrete is used for casting all arch ribs. and the bridge construction layout is shown in Figure 6.

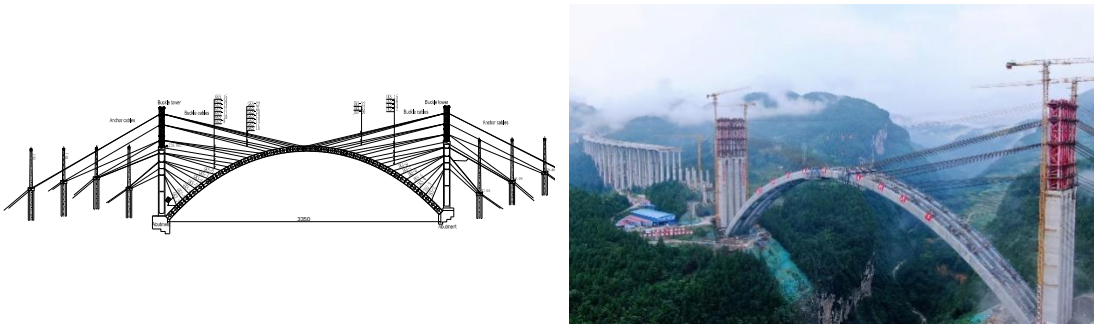

(a) (b)

Figure 6 Bridge layout and site monitoring. (a) Layout of bridge type. (b) Construction site monitoring.

The numerical calculation model of RC arch bridge structure was established by finite element software. The eight-node SOLID65 element was used to simulate the concrete main arch ring and junction pier, the LINK180 element for fasteners and anchor cables, and beam elements for arch columns and main girders. The entire bridge was meshed using a combination of mapping and sweeping methods. Figure 7 presents the finite element model.

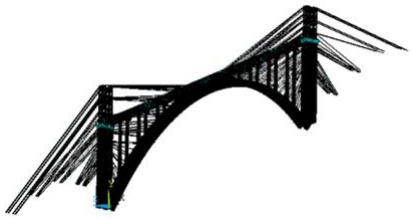

Figure 7 Finite element model.

5.2 Algorithm performance testing

To validate the performance of the improved strategy in seeking optimal solutions as presented in this study, 6 types of CEC benchmark test functions are selected to illustrate, including 3 single-peak multi-dimensional test functions and 3 multi-peak multidimensional test functions. The optimization performance of the improved Gray Wolf algorithm in this study is compared with GWO, WOA and DBO algorithms, and the test functions are listed in Table 1.

Table 1 Test function basic information.

Function number	Function name	The theoretical optimal solution
f_1	Sphere	0
f_2	Step function	0
f_3	Quartic noise function	0
f_4	Ackely	0
f_5	Generalized Griewank function	0
f_6	Generalized penalty function	0

Each algorithm operates with a population of 30 and a maximum of 500 iterations. It is independently run 30 times on the test function. The optimization performance of each algorithm is evaluated by comparing the optimal, average, and standard deviation values of the test functions calculated by each algorithm. The optimization results are presented in Table 2.

From Table 2, the IGWO algorithm in this study has reached the theoretical optimal solution in two single-peak test functions and one multi-peak test function, and the standard deviation of the five test functions is 0. Although IGWO did not obtain the theoretical optimal solution for the remaining one single-peak and two multi-peak test functions, its obtained optimal values are closer to the theoretical

optimum than those of the other three optimization algorithms, with the average optimal values serving as a reference. For the Ackley function, although the optimal value obtained by the proposed IGWO is comparable to those of other algorithms, its standard deviation is zero, indicating that the Levy flight strategy and nonlinear attenuation factor introduced in this study enhance the algorithm's stability, strengthen its global search capability, and prevent it from falling into local optima. These results demonstrate that the IGWO algorithm outperforms other optimization algorithms in convergence accuracy and stability when solving both single-peak and multi-peak function problems.

Table 2 Optimization test results.

Function number	Algorithm name	Optimal value	Mean value	Standard deviation
f_1	WOA	6.2×10^{-18}	2.1×10^{-11}	7.3×10^{-11}
	DBO	7.7×10^{-29}	9.2×10^{-17}	2.2×10^{-17}
	GWO	9.5×10^{-16}	1.8×10^{-15}	2.5×10^{-15}
	IGWO	0	0	0
f_2	WOA	5.6×10^{-2}	5×10^{-1}	3×10^{-1}
	DBO	9.1×10^{-5}	9.3×10^{-3}	4.6×10^{-2}
	GWO	2.5×10^{-1}	5.1×10^{-1}	3.4×10^{-1}
	IGWO	0	0	0
f_3	WOA	1.5×10^{-5}	4.6×10^{-3}	5.7×10^{-3}
	DBO	3.2×10^{-5}	3.1×10^{-3}	3.2×10^{-3}
	GWO	4.9×10^{-4}	2.2×10^{-3}	1.3×10^{-3}
	IGWO	7.8×10^{-6}	7.1×10^{-5}	1.5×10^{-5}
f_4	WOA	2.5×10^{-15}	2.4×10^{-14}	1.8×10^{-14}
	DBO	1.5×10^{-16}	1.5×10^{-16}	0
	GWO	3.5×10^{-15}	4.2×10^{-14}	2.5×10^{-15}
	IGWO	1.3×10^{-16}	1.3×10^{-16}	0
f_5	WOA	0	2.1×10^{-2}	4.9×10^{-2}
	DBO	0	0	0
	GWO	0	7×10^{-3}	1.8×10^{-2}
	IGWO	0	0	0
f_6	WOA	4×10^{-6}	2.8×10^{-6}	2.3×10^{-5}
	DBO	7.3×10^{-7}	1.4×10^{-5}	3.2×10^{-5}
	GWO	1.2×10^{-6}	5.1×10^{-6}	3.5×10^{-6}
	IGWO	1.7×10^{-25}	1.7×10^{-25}	0

To validate the improved convergence speed of the proposed IGWO algorithm, this study presents the comparison results of the convergence curves of the four algorithms for the test functions, as shown in Figure 7. For f_3, f_4 and f_6 test functions, a while neither IGWO nor the other algorithms converge to the theoretical optimal solution, IGWO exhibits faster convergence speed, approaches the theoretical optimum more closely in later iterations, and achieves better convergence accuracy, confirming the improvement in its convergence speed.

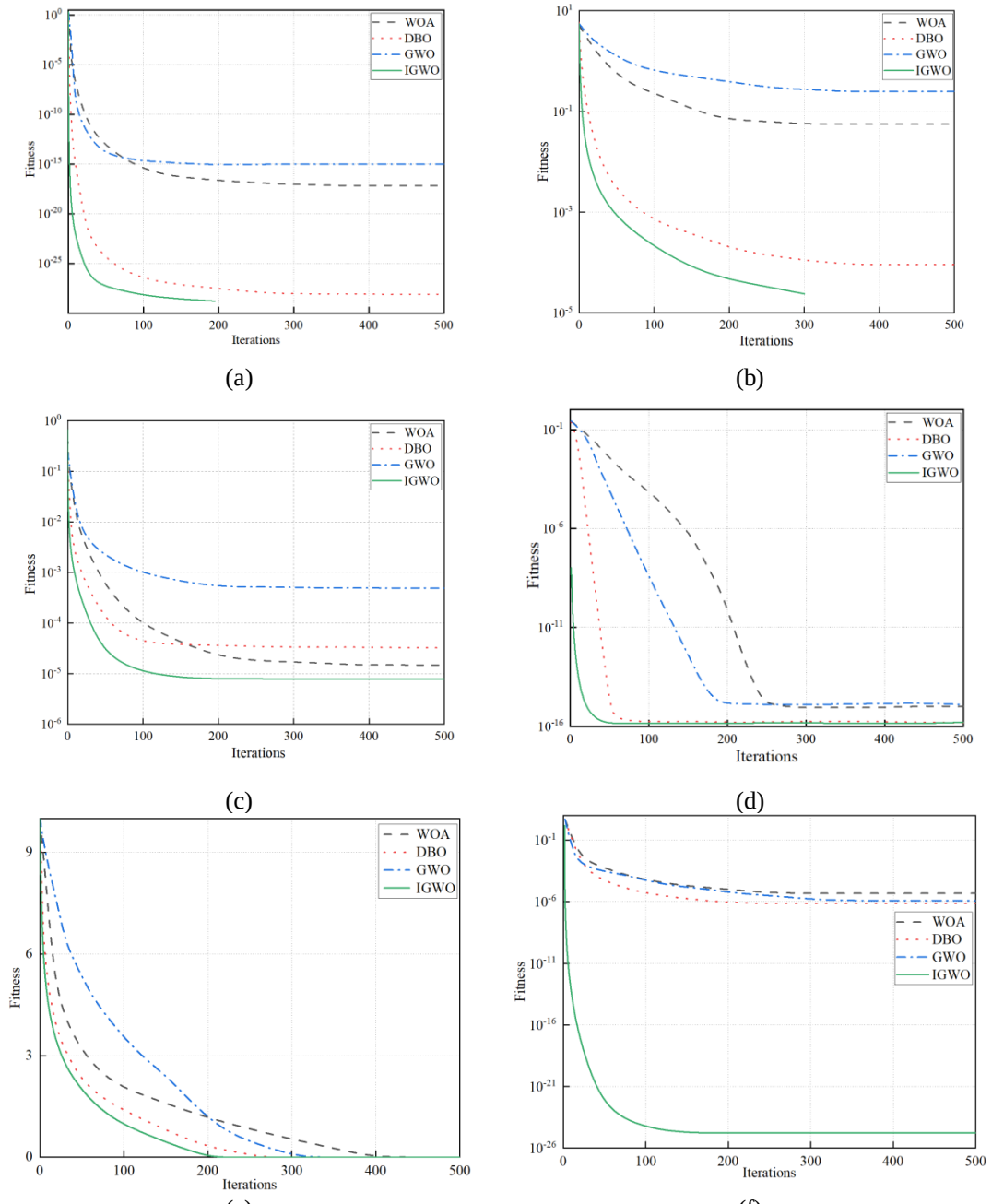

Figure 8 Comparison results of convergence velocity curves. (a) f1 iterative curve. (b) f2 iterative curve. (c) f3 iterative curve. (d) f4 iterative curve. (e) f5 iterative curve. (f) f6 iterative curve.

5.3 Surrogate mode accuracy verification

According to the process mentioned previously, the Kriging surrogate model was built. To validate the prediction precision of the surrogate model, the complex correlation coefficient R^2 was utilized to demonstrate. Figure 9 depicts the convergence history of the multi-objective optimization for the Kriging surrogate model. The multiple correlation coefficients R^2 corresponding to the three optimization objectives are all greater than 0.98, indicating that the accuracy of the 7th-generation Kriging surrogate mode meets the requirements. At the same time, to guarantee the precision and dependability of the model, verification points are set for explanation [23-26], and the number of verification points is consistent with the output variables, set to 3. The nearer the point set approaches the y = x line, the more ideal the model's fitting effect will be. The fitting results are shown in Figure 10. The verification points of the three objective functions are highly coincident with the y=x lines, which indicates that the model has high fitting accuracy in these three output variables. In summary, the proxy model proposed in this study can be used to calculate the cable force optimization for RC arch bridges.

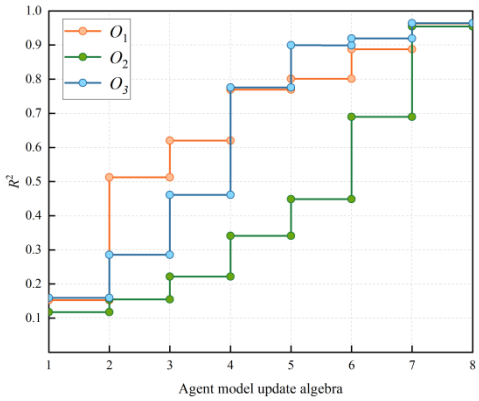

Figure 9 Kriging proxy model multi-objective optimization convergence journey.

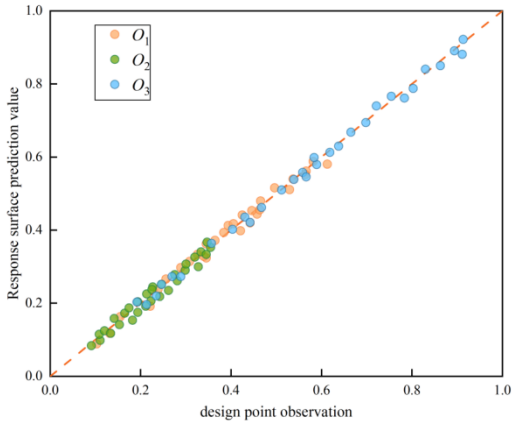

Figure 10 Fitting curve

Figure 11 shows the partial structural response surface fitted according to the Kriging model. By examining the bridge structural response surface, the Kriging model is demonstrated to effectively fit the bridge's structural response characteristics. The response surface is smooth, and the fitting effect is favorable.

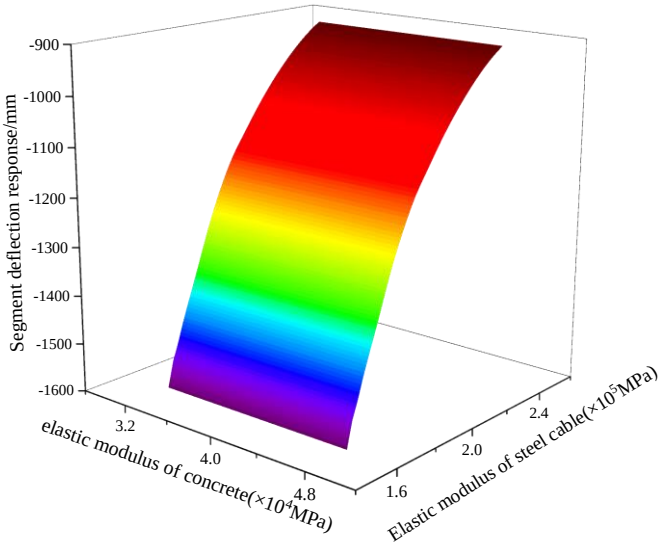

Figure 11 Kriging response surface.

Based on the proposed IGWO in this study, the Pareto frontier solution set for the multi-objective optimization of O_1, O_2 and O_3 is obtained, as shown in Figure 12. The figure illustrates that this study involves three optimization objectives, with the Pareto frontier solution set distributed in a three-dimensional space. With the optimization iteration, Pareto frontier solution set approaches to the minimum values of O1, O2 and O3, and basically converges when iteration reaches the 50th time.

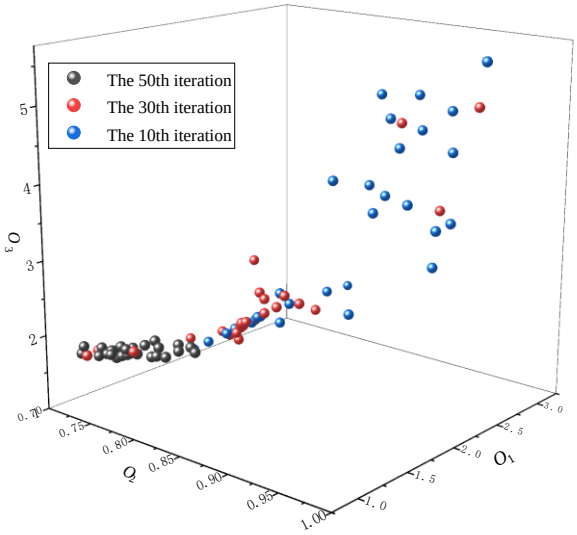

Figure 12 Pareto frontier solution set.

5.4 Optimization analysis of tension

When analyzing the results of cable force optimization, since only half structure is selected for research in Section 4.2, Figure 13 shows the comparison before and after cable force optimization. The figure clearly demonstrates that the distribution trends of the cable forces before and after optimization are essentially consistent, with the optimized values exhibiting varying degrees of increase compared to the originally designed cable forces. Among them, the cable force value at the arch foot increases slightly, while the cable force value at the middle position and the crown position increases greatly, and the 15# cable has the most significant increase, about 12.1%. Based on the analysis of the mechanical characteristics of the RC arch bridge cantilever, as construction progresses, the horizontal angle between the cable and the arch ring segment increases; simultaneously, the vertical component of the cable force decreases while its horizontal component increases. Therefore, the increase in the optimized cable force provides more vertical component for each arch ring during cantilever pouring, thereby preventing the vertical component from being insufficient—caused by the increased horizontal angle—from compromising the arch ring's stability and ensuring construction safety.

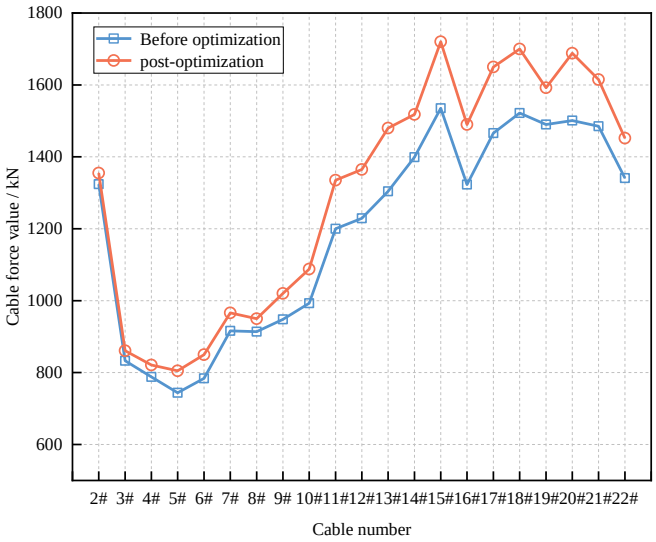

Figure 13 Cable force optimization results.

As shown in Figure 14, which compares the peak tensile stresses in each arch segment before and after optimization, the top and bottom plates of all segments exhibit a significant reduction in peak tensile stress post-optimization. The decrease is particularly pronounced in the top plates of mid-arch segments,

whereas the reductions in the arch crown and springing segments are relatively modest. For Segments #10–#11, top plate peak tensile stress decreased by over 40% after optimization. Specifically, Segment #11's peak tensile stress dropped from 3.38 MPa (pre-optimization) to 1.89 MPa, representing a reduction of approximately 44.1%. Additionally, substantial declines were observed in the bottom plate peak tensile stresses of all segments, with Segment #13 experiencing the most significant reduction of about 67.3%. Following cable force optimization, peak tensile stresses in all arch segments of the reinforced concrete arch bridge remained below the design tensile strength of C80 concrete, thus fulfilling the optimization objectives.

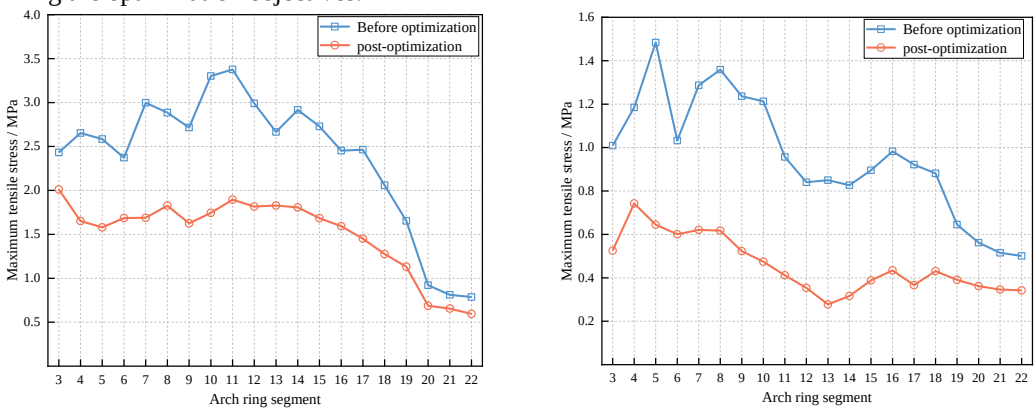

(a) (b)

Figure 14 Optimization results of peak tensile stress of each section of the arch ring. (a) Peak tensile stress of arch segment roof. (b) Peak tensile stress of arch ring segment floor.

Figure 15 illustrates the bending moment and axial force values of the arch ring in the completed-bridge state before and after cable force optimization. As depicted, the internal force distribution trends remain largely consistent before and after optimization, though both bending moments and axial forces at various arch ring sections show varying degrees of reduction. Specifically: The arch foot bending moment decreases from 37,991.8 kN·m to 34,327.9 kN·m, a reduction of approximately 9.6%. The arch crown bending moment decreases from 62,786.9 kN·m to 54,737.7 kN·m, a reduction of approximately 12.8%. The arch foot axial force decreases from 79,821 kN to 79,155.8 kN, a reduction of approximately 0.8%. The arch crown axial force decreases from 67,774 kN to 66,960.9 kN, a reduction of approximately 1.2%. Following optimization, the RC arch bridge's internal force distribution under dead load is more reasonable, fulfilling the optimization objectives.

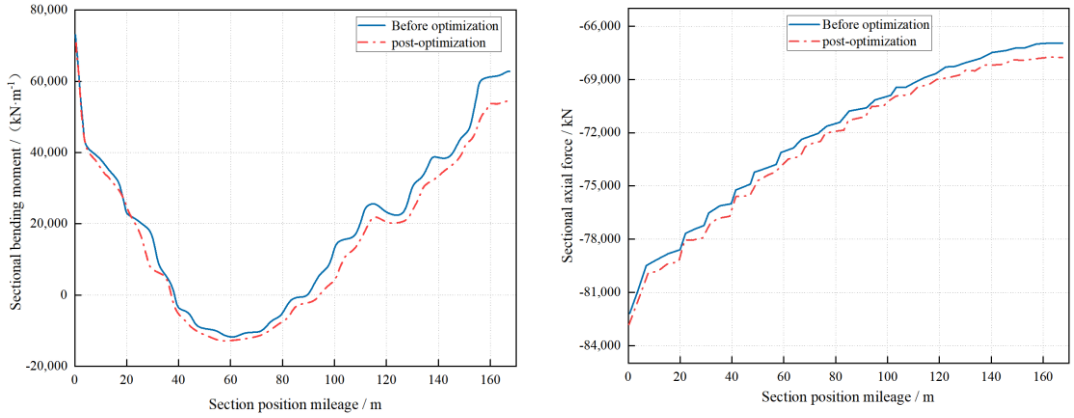

(a) (b)

Figure 15 Internal force optimization results of arch bridge. (a) Bending moment optimization results. (b) Axial force optimization results.

Figure 16 shows that the vertical displacement of the RC arch bridge's main arch ring decreases significantly after cable force optimization. Because the position constraint of arch foot is large and the vertical displacement is small, the displacement re-duction after cable force optimization is not significant. During the cantilever pouring process, as the cable length increases, the cable force rises correspondingly. Moreover, at the closing section, the vertical force supplied by the cable force is

relatively minimal, and it is precisely at this moment that the vertical displacement reaches its maximum value. After optimization, the vertical deformation of the arch top position decreased from 15.94 cm to 12.83 cm after optimization, with a decrease of about 19.5%. The overall linear distribution of the arch ring was more reasonable than before optimization, which greatly improved the overall safety and reliability performance of the RC arch bridge structure and met the optimization objectives.

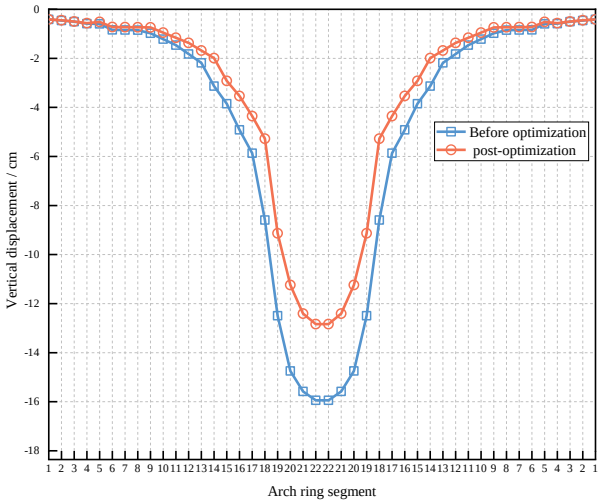

Figure 16 Optimization results of the vertical displacement of each segment of the arch ring.

6. Conclusions

To tackle the challenge of optimizing cable force during the cantilever casting of RC arch bridges, this study proposes a multi-objective cable force optimization method based on Kriging-IGWO. Multiple strategies are introduced to enhance the traditional Grey Wolf Optimization algorithm. Leveraging the Kriging surrogate model and multi - objective optimization theory, a multi - objective cable force optimization model for reinforced concrete arch bridges is developed, from which the following conclusions are derived: The following conclusions are obtained:

(a) By incorporating the Levy flight strategy, nonlinear attenuation strategy, and dynamic weight coefficient strategy to enhance the traditional Gray Wolf Optimizer (GWO), the IGWO algorithm is verified by six benchmark test functions to exhibit superior convergence accuracy, better stability, and significant advantages in solving complex function optimization problems.

(b) A Kriging surrogate model was constructed to fit the structural response surface of the RC arch bridge. After the seventh update, the multiple correlation coefficients R^2 for the multi-objective optimization all exceeded 0.98. The model's predicted values aligned well with the design points overall, and the verification points of the three objective functions lay close to the y=x line, demonstrating that the model exhibits high fitting accuracy for these three output variables. It can effectively predict the structural response, providing reliable support for the cable force optimization of the cantilever-poured RC arch bridge structure.

(c) Based on the Kriging-IGWO cable force optimization model, the cable forces of the RC arch bridge were optimized. After optimization, the cable force distribution trend remained consistent with the original design, though the cable force values increased. The peak tensile stresses in the top and bottom plates of each arch ring segment decreased significantly, all falling below the design tensile strength of C80 concrete. The internal force distribution trend remained basically unchanged, yet the bending moments and axial forces of each arch ring segment were reduced to varying degrees. The vertical displacement of the main arch ring decreased notably: the arch crown displacement dropped from 15.94 cm to 12.83 cm, a reduction of approximately 19.5%. The arch ring's deformation distribution became more reasonable, enhancing the overall safety and reliability of the bridge structure and fulfilling the optimization objectives.

Data Sharing Agreement

The datasets used and/or analyzed during the current study are available from the corresponding author on reasonable request.

Competing Interests

The authors have no relevant financial or non-financial interests to disclose.

Acknowledgment

This article was supported by the National Nature Science Foundation of China (grant number :52078058), the National Nature Science Foundation of China(grant number : 51478049), and the Sichuan Provincial Transportation Technology Project(grant number 2021-ZL-07).

References

[1] Jiapeng, S.; Yu, T.; Qingyun, X.; Jie, D.; Jin, D.; Fengjiang, Q.Optimization of Reasonable Finished State for Cable-Stayed Bridge with Steel Box Girder Based on Multiplier Path Following Method.*Applied Sciences*.**2025,15**,937-937.

[2] Wang, L.; Zhang, Y.; Liu, X. L.. A tensioning control method for stay cables with super large tonnage cable force. *International journal of structural integrity*. **2024** ,15, 613-630.

[3] Cheng, J.; Yuan, Y.; Yu, Z.; Sun, K. Estimation of the anti-sliding safety factor between the main cable and middle saddle of three-pylon steel suspension bridges. *International Journal of Steel Structures*. **2024**, 24, 709-718.

[4] Li, Z.; Bowen, M.; Xuejin, H.; Wei, L. Cable force optimization of cable-stayed bridges based on the influence matrix and elite genetic algorithm. *Journal of Southeast University* (*English Edition*). **2024**,40,129-139.

[5] Zhou, X.; Cao, L.; Xie, W.; Qin, D. DNN surrogate model based cable force optimization for cantilever erection construction of large span arch bridge with concrete filled steel tube. *Advances in Engineering Software*.**2024**, 189, 103588-103599.

[6] Huizhong, X.; Xin, Y.; Yongnan, H.; Yong, H. Optimization of cable-stayed force for asymmetric single tower cable-stayed bridge formation based on improved particle swarm algorithm.*International Journal of Structural Integrity*.**2024**,15,873-901.

[7] Guo, J.; Yuan, W.; Dang, X.; Alam, M. S. Cable force optimization of a curved cable-stayed bridge with combined simulated annealing method and cubic b-spline interpolation curves. Engineering Structures.**2019**, 201, 109813.1-109813.11.

[8] Tian, Z.; Zhang, Z.; Ning, C.; Peng, T.; Guo, Y.; Cao, Z. Multi-objective optimization of cable force of arch bridge constructed by cable-stayed cantilever cast-in-situ method based on improved NSGA-II. *Structures*.**2024**, 59, 105782-.

[9] Cao, H.; Li, H.; Zhou, Y.; Li, Z.; Feng, L. Biobjective optimization of cable force for concrete cable-stayed bridges considering the requirements of the serviceability and ultimate limit state. *Journal of Bridge Engineering.* **2024**, 29, 13.

[10] Wang, Z.; Zhang, N.; Du, X.; Wang, S.; Sun, Q. Multiobjective optimization of cable forces and counterweights for universal cable-stayed bridges. *Journal of Advanced Transportation*.**2021**, 1,1-13.

[11] Reyes-Sierra, M.; Coello, C. C. A. Multi-objective particle swarm optimizers: a survey of the state-of-the-art. *International Journal of Computational Intelligence Research*.**2006**, 2, 287-308.

[12] Zhangming, W.; Nan, Z.; Qian, C. Multi-objective optimization-based reasonable finished state in long-span cable-stayed bridge considering counterweights.*Structures*.**2023**,51,1497-1506.

[13] Guo, L.; Zhang, Z. .; Wu, T.; Zeng, Y.; Zhang, Y.; Xie, X. A grey wolf optimization algorithm for solving partial destructive disassembly line balancing problem consider feasibility evaluation and noise pollution. *Advanced engineering informatics*. **2024**,60, 102418-.

[14] Mirjalili, S.; Mirjalili, M, S.; Lewis, A. Grey Wolf Optimizer .*Advances in Engineering Software*.**2014**,69,46-61.

[15] Liu, Y.; As'Arry, A.; Hassan, M. K.; Hairuddin, A. A.; Mohamad, H. Review of the grey wolf optimization algorithm: variants and applications. *Neural Computing & Applications*.**2024**, 36, 2713-2735.

[16] Xiujian, Y.; Jinlin, Gan. Optimisation of commercial bus body frame based on the improved grey wolf and Monte Carlo simulation algorithm. *International Journal of Vehicle Performance*.**2024**,10,24-49.

[17] Fan, Z.; Huang, C.; Gao, J.; Zhang, K.; Xu, Z.; Fan, M. Prediction of liquid bridge rupture between two plates combining artificial neural network with grey wolf optimization algorithm. *Granular Matter*. **2025**, 27, 1-16.

[18] Wang, H. Predicting the compressive strength of high-performance concrete employing multi-composed radial-based neural network. *Multiscale and Multidisciplinary Modeling, Experiments and Design* . **2024**, 7, 1925-1940.
[19] Lorand, C.; Bouet, Léa.; Devineau, O.; Chimienti, M.; Evans, A. L.; Callahan, P. A supervised model to identify wolf behavior from tri-axial acceleration. *Animal Biotelemetry*. **2025**, 13, 1-13.
[20] Miura, H. A study of travel time prediction using universal kriging. *TOP*. **2010**,18, 257-270.
[21] Li, D.; Ye, Z.; Lu, P.; Wu, Y.; Yang, L.; Wang, J. Reliability intelligence analysis of concrete arch bridge based on kriging model and PSOSA hybrid algorithm. Artificial Intelligence Review. **2023**,56,2667-2685.
[22] Peralta-Braz, P.; Alamdari, M. M.; Hassan, A. M. On the joint optimization of energy harvesting and sensing of piezoelectric energy harvesters: case study of a cable-stayed bridge. *IEEE transactions on intelligent transportation systems*.**2024**, 25, 559-570.
[23] Wang, J.; Cao, Z.; Xu, G.; Yang, J.; Kareem, A. An adaptive kriging method based on k-means clustering and sampling in n-ball for structural reliability analysis. *Engineering Computations.* **2023** ,40, 378-410.
[24] Zhong, J.; Zheng, X.; Zhu, Y.; Dang, X. Resilience-based seismic design optimization of novel link beam in a double-column bridge bent using gaussian process regression. *Bulletin of Earthquake Engineering*.**2023**,21,6121-6142.
[25] Zhong, W.; Chen, Z.; Chen, C.; Liu, C.; Li, M.; Wang, J. An ego-based online model updating method for hybrid simulation. *Engineering Structures.* **2024**, 307,117955-.
[26] Chen, C.; Long, J.; Chen, W.; Liu, Z.; Guo, J. Modeling and prediction of spindle dynamic precision using the kriging-based response surface method with a novel sampling strategy. *Nonlinear Dynamics*. **2023**, 111, 559-579.